Random-bond Potts model in the large-q limit

Róbert Juhász,[1,2] Heiko Rieger,[3] and Ferenc Iglói[2,1,4]
[1]*Institute for Theoretical Physics, Szeged University, H-6720 Szeged, Hungary*
[2]*Research Institute for Solid State Physics and Optics, P.O. Box 49, H-1525 Budapest, Hungary*
[3]*Theoretische Physik, Universität des Saarlandes, 66041 Saarbrücken, Germany*
[4]*Centre de Recherches sur les Trés Basses Températures, Boîte Postale 166, F-38042 Grenoble, France*
(Received 12 June 2001; published 24 October 2001)

We study the critical behavior of the q-state Potts model with random ferromagnetic couplings. Working with the cluster representation the partition sum of the model in the large-q limit is dominated by a single graph, the fractal properties of which are related to the critical singularities of the random-Potts model. The optimization problem of finding the dominant graph, is studied on the square lattice by simulated annealing and by a combinatorial algorithm. Critical exponents of the magnetization and the correlation length are estimated and conformal predictions are compared with numerical results.

DOI: 10.1103/PhysRevE.64.056122 PACS number(s): 05.50.+q, 64.60.Fr, 75.10.Nr

I. INTRODUCTION

The effect of quenched disorder at a first-order transition point is comparatively less understood than the same phenomena at a continuous transition point. In the latter case relevance-irrelevance criteria, such as the Harris criterion [1,2] can be used to decide upon the stability of the pure fixed point and also perturbation expansions are developed [3] to treat the effect of weak disorder. If the transition in the pure system is of first order, neither a general relevance criterion nor a consistent perturbation expansion is known to apply around the discontinuity fixed point of the pure model. One remarkable exception is the stability criterion by Aizenman and Wehr [4] (based on an idea of Imry and Wortis [5], see also by Hui and Berker [6]), which rigorously states that in two dimensions (2D) any amount of quenched disorder will soften the first-order transition in the pure system into a continuous one. In 3D the same criterion predicts a crossover phenomenon, generally the transition stays discontinuous for weak disorder, whereas it turns to a second-order transition for sufficiently strong disorder [7].

Based on the above rigorous results intensive numerical work has started to clarify the universality class of different disordered models, which have a discontinuous transition in their pure form. In 2D most of the work has been devoted to the q-state Potts model, for which the transition point is known from self-duality also in its disordered version [8], and in the pure model exact result by Baxter [9] ensures a first-order transition for $q>4$. Although early Monte Carlo (MC) simulations [10] left space for an interpretation [11] of a q-independent superuniversal behavior in random systems, later extensive MC [12] and transfer matrix [13] calculations consistently determined q-dependent magnetic exponents, whereas the correlation length exponent, ν, was found to be close to the pure Ising value, $\nu_I=1$, for all q.

In the large-q limit thermal fluctuations are reduced and as a consequence the pure model is soluble in any dimension and a perturbation expansion in powers of $1/q^{1/d}$ can be performed. In the same limit for the random model at the phase transition point an effective interface Hamiltonian has been constructed and mapped onto the interface Hamiltonian of the random-field Ising model (RFIM) [13]. This mapping has then been used to relate the phase diagram of the two problems and to deduce the tricritical exponents of the random-bond Potts model (RBPM) at $d>2$ dimensions. However, in the large-q limit no *direct* calculation to study the critical behavior has yet been performed. In 2D the presently known information is obtained via extrapolation of the results calculated at finite values for q. From these estimates no special type of critical behavior is expected in the large-q limit. For example the magnetization scaling dimension, x_m, seems to saturate at a finite, nontrivial limiting value [14,15] $\lim_{q\to\infty} x_m(q)\approx 0.17-0.19$. However, at this point one should note on the presence of strong (logarithmic) corrections in the form of $1/\ln q$, see cf. Fig. 5 in Ref. [14].

In the present paper we are going to perform a direct investigation of the critical behavior of the RBPM in the large-q limit. As will be shown, in that limit the thermal fluctuations are negligible and the calculation of the average thermodynamical and correlation properties of the model is effectively reduced to an optimization problem. Here the competition between ordering effects, originating from a tendency to clustering, and disordering effects, due to energy gain from quenched disorder, plays an important role in determining the optimal structure. In two dimensions we perform a numerical study based on simulated annealing and a combinatorial algorithm, and also conformal aspects of the problem are investigated.

The structure of the paper is the following. In Sec. II we introduce the random cluster representation of the Potts model and define the equivalent optimization problem emerging in the large-q limit. Results obtained from the solution of the optimization problem in different 2D geometries are presented in Sec. III and discussed in Sec. IV.

II. CLUSTER REPRESENTATION IN THE LARGE-q LIMIT

We consider the q-state Potts model on a d-dimensional hypercubic lattice with periodic boundary conditions defined by the Hamiltonian

$$\frac{H}{kT} = -\sum_{\langle ij \rangle} K_{ij} \delta(\sigma_i, \sigma_j), \tag{2.1}$$

where σ_i are q-state Potts variables ($\sigma_i \in \{1, \ldots, q\}$ located at lattice sites i, the sum goes over all nearest neighbor pairs $\langle ij \rangle$ of the lattice, and $K_{ij} > 0$ are reduced ferromagnetic couplings. The d-dimensional hypercubic lattice corresponds to a graph $\overline{G} = (V,E)$, where V is the set of vertices, which is identical to the lattice sites, and E is the set of edges, which is identical with the bonds between neighboring sites on the lattice. In the random cluster representation [16] the partition sum of the model, Z, is expressed as a sum over all subsets $U \subseteq E$ of the set of edges (or bonds) as

$$Z = \sum_{U \subseteq E} q^{n(U)} \prod_{(ij) \in U} v_{ij}, \tag{2.2}$$

where $n(U)$ denotes the number of connected clusters in the subgraph $G = (V,U)$ of $\overline{G}$, consisting of all lattice sites but the reduced set of bonds in U, and $v_{ij} = e^{K_{ij}} - 1$ is the Mayer function for the coupling K_{ij}. For the latter we use the parameterization

$$v_{ij} = q^{1/d + w_{ij}}. \tag{2.3}$$

Then the contributions from the different graphs to Z are expressed in powers of q,

$$Z = \sum_{U \subseteq E} q^{F(U)} \tag{2.4}$$

with

$$F(U) = n(U) + \sum_{(ij) \in U} \left(\frac{1}{d} + w_{ij} \right). \tag{2.5}$$

In the following we consider the large-q limit ($q \to \infty$), where the partition sum is dominated by the leading term given by the maximum value for F,

$$F_0 = \max_{U \subseteq E} \{F(U)\}, \tag{2.6}$$

where $-F_0$ corresponds to the free energy of the system up to a prefactor of $1/(kT \ln q) = \text{const}$. Let us denote with U_0 the subset of E that gives the optimum in Eq. (2.6), i.e., $F_0 = F(U_0)$, and with $G_0 = (V,U_0)$ the corresponding *dominant graph*. Then the energetic contribution to $-F_0$ is due to the couplings in the dominant graph, whereas the entropic term is related to the number of connected parts. In what follows, we use the word graph when we mean the subgraph $G = (V,U)$ of $\overline{G}$ defined by an edge subset U.

In the pure system, with $w_{ij} = w$, the structure of the dominant graphs in the different thermodynamic phases are trivial. Consider a lattice with $N = L^d$ spins with fully periodic boundary conditions, the number of bonds is dN. Then, in the low-temperature phase with $w > w_c$ the *fully connected graph* (V,E) is the dominant graph, thus $F_0 = F_c = [dN(1/d + w) + 1]$. On the other hand, in the high-temperature phase, $w < w_c$, the dominant contribution is due to the *empty graph* $(V,\varnothing)$, with a value of $F_e = N$. At $w_c = -1/dN$, when $F_c = F_e$, there is phase coexistence, which means a sharp phase transition even in a finite system in the limit of $q \to \infty$. In the thermodynamic limit we have $w_c = 0$, and the latent heat per site is given by $\Delta L/N = 1$ in our units.

Introducing disorder, such that w_{ij} can take randomly positive and negative values, the question arises, whether this trivial structure of the dominant graph persists at the transition point, i.e., is there still a coexistence between two parts of the graph, one being fully connected, whereas the other is empty? To study this problem Cardy and Jacobsen [13] have constructed the interface Hamiltonian, which is then mapped onto that of the RFIM. This has lead to the answer that for $d > 2$ the effect of small disorder is irrelevant, thus there is still phase coexistence and thus the transition is of first order, whereas in $d = 2$ the phase coexistence is destroyed by any amount of disorder, in accordance with Aizenman and Wehr exact results [4].

In the following we are going to consider the problem in 2D where the dominant graph has a nontrivial structure. In particular we study the (fractal) properties of the largest connected cluster of G_0, denoted by Γ. In the low-temperature phase, $T < T_c$, Γ is compact, thus the average number of points in Γ is given by $[n_\Gamma]_{\text{av}} \propto N = L^2$, where L is the linear size of the square lattice and here and in the following $[\cdots]_{\text{av}}$ denotes the average over the quenched disorder. In the high-temperature phase, for $T > T_c$, $[n_\Gamma]_{\text{av}}$ stays finite and defines the average correlation length, ξ, through $[n_\Gamma]_{\text{av}} \sim \xi^2$. At the transition point the average mass is expected to scale as

$$[n_\Gamma]_{\text{av}} \sim L^{d_f}, \tag{2.7}$$

with an average mass exponent $d_f < 2$ [17].

The properties of $[n_\Gamma]_{\text{av}}$ are directly related to the asymptotic behavior of the average spin-spin correlation function, defined in the large-q limit as

$$[C(r)]_{\text{av}} = [\langle \delta(\sigma_i, \sigma_j) \rangle]_{\text{av}}, \tag{2.8}$$

where $\langle \cdots \rangle$ denotes the thermal and spatial average over all pairs of sites i and j with a distance r. We use the fact that correlations between two spins are generally zero, unless they belong to the same cluster, when $C(r) = 1$. In the case of $T \leqslant T_c$, when Γ is a spanning cluster the probability, $P(L)$, that a spin belongs to Γ is given by $P(L) = [n_\Gamma]_{\text{av}}/N$, whereas the same probability for two spins is $P(L)^2$. From this follows, that the average correlations between two spins separated by a large distance of $r = L$ is given by $[C(r)]_{\text{av}} \simeq P(L)^2 = ([n_\Gamma]_{\text{av}}/N)^2$. In the low-temperature phase, $T < T_c$, where the average magnetization, $[m]_{\text{av}}$, is defined as $[m]_{\text{av}}^2 = \lim_{r \to \infty} [C(r)]_{\text{av}}$, we obtain

$$[m]_{\text{av}} = \lim_{L \to \infty} \frac{[n_\Gamma]_{\text{av}}}{L^2}, \quad T < T_c, \tag{2.9}$$

whereas at the critical point the average spin-spin correlations decay as a power

$$[C(r)]_{\text{av}} \sim r^{-2x_m}, \quad x_m = 2 - d_f, \quad T = T_c. \tag{2.10}$$

Finally, in the high-temperature phase, where the average size of Γ is finite the probability to have a connected cluster of size r is exponentially small, which leads to an average correlation function of the form $[C(r)]_{\rm av} \sim \exp(-r/\xi)$, for $r \gg \xi$.

In the following we specify the form of the disorder, where we make use of the simplification that arises due to self-duality that holds under special conditions. According to the results by Kinzel and Domany [8] the random model is at the critical point, if the distribution, $P(w)$, of w_{ij} is an even function of w, thus $P(w)=P(-w)$. For convenience we use the bimodal distribution,

$$P(w)=p\,\delta(w-\omega)+(1-p)\,\delta(w+\omega), \qquad (2.11)$$

where the critical point is at $p=p_c=1/2$, whereas the reduced temperature, $t=(T-T_c)/T_c$, can be expressed as

$$t=-\omega(p-1/2), \quad |t| \ll 1. \qquad (2.12)$$

Generally we restrict ourselves to the range of disorder parameterized as $0<\omega<1/2$. We note that for $\omega=0$ one recovers the pure model, whereas for $\omega>1/2$ we are in the usual percolation limit. Indeed, for the latter range of parameters the dominant graph contains all the strong bonds, whereas the weak bonds are all absent.

III. METHODS AND RESULTS

According to the results presented in the previous section the solution of the RBPM in the large-q limit is equivalent to an optimization problem with a nonlocal cost function given by Eq. (2.5). To find the dominant graph of the problem we used standard approximative procedures. Most of the results were obtained by the method of simulated annealing, but some calculations were performed by an approximative combinatorial optimization algorithm.

In the procedure of simulated annealing a hypothetical temperature variable, T_h, is introduced and, after thermalization, is lowered until the hopefully global minimum of the cost function is reached. In practical applications we lowered the temperature as $T_h=1/(\tau-0.5)$, in finite time steps $\tau=1,2,\ldots,60$, and checked that the resulting configuration does not change after further cooling. At a fixed temperature in the thermalization MC steps we generally used local rules by creating or removing bonds, but sometimes we also considered to move a full line of bonds. In order to arrive to the global minimum several different starting configurations are considered (at least three, sometimes several hundred), and the best final configuration was taken. In the investigations generally $L\times L$ finite samples with linear size up to $L=24$ were considered and periodic boundary conditions were used in both directions. For smaller sizes the averaging was usually performed over 10 000 samples, whereas for larger sizes we used several thousands of realizations.

Alternatively, for small ω (precisely for $\omega<0.25$) we used a combinatorial optimization algorithm that yields a configuration that is close to the optimum but not necessarily equal to it. Actually the worst case bound for the ratio of the value F_0 of the optimal solution U_0 is to the value $F(U)$ configuration U that is found by the algorithm is only 2/3, which would be too bad for our purposes. However, in typical cases the configurations produced by the algorithm are much closer, as we checked by comparison with the configurations generated by the simulated annealing method. The algorithm works as follows [18].

For all sites i let i_{x-}, i_{x+}, i_{y-}, and i_{y+} be its left, right, lower, and upper neighbor, respectively, and denoted with (ii_{x-}), (ii_{x+}), (ii_{y-}), and (ii_{y+}) the bonds (edges) between these neighboring sites and i. These constitute a minimal set of edges that, when removed from $\overline{G}$ cut the site i from the rest of the graph. Let us denote them by

$$E_i=\{(ii_{x-}),(ii_{x+}),(ii_{y-}),(ii_{y+})\} \qquad (3.1)$$

and their weight

$$w(E_i)=\sum_{(ij)\in E_i}\left(\frac{1}{2}+w_{ij}\right). \qquad (3.2)$$

The minimum cut between any two pairs of sites, i and j, (i.e., the set of edges that has a minimum total weight *and* whose removal from $\overline{G}$ cuts the graph into two disjoint subgraphs, one containing i and other j) is then given either by E_i or E_j, as long as $|w_{ij}|<1/4$, as one can easily convince oneselves.

The idea of the algorithm is as follows. Obviously the removal of the edges contained in a minimum cut, such as in E_i for all i, increases the number of components in the graph by one, i.e., one wins one unit in the cost function $F(U)$, Eq. (2.5). On the other hand, one loses $w(E_i)$ units and when increasing the number of components of the graph G one should keep this weight loss as small as possible. Therefore we consider a collection of minimum cuts as possible candidates of edge sets to be removed from $\overline{G}$.

Let the edge sets be ordered nondecreasing weight, such that $w(E_1)\leqslant w(E_2)\leqslant\cdots\leqslant w(E_{L^2})$ and define for all $r=0,1,2,\ldots,L^2$ the edge subsets

$$U_r=E\setminus\bigcup_{i=1}^{r}E_i, \qquad (3.3)$$

i.e., $U_0=E$, and with increasing r successively edge sets of nondecreasing weight are substracted from E. When doing this initially (i.e., for small r) most of the time a site will be isolated that has been connected before to a larger cluster and therefore frequently (depending on the weight of the substraced edges) $F(U)$ will increase, as desired. These are the trial configurations for our optimization problem and we take the best solution among them, i.e., U^* such that $F(U^*)=\max\{F(U_r)|r=0,1,\ldots,L^2\}$. It can be shown [18] that $F(U^*)/F(U_{op})\geqslant 2/3$, where U_{op} is the exact optimal solution of Eq. (2.6). With the combinatorial optimization method we could treat larger finite systems (up to 128×128), than by simulated annealing and the number of configurations we used were between 10 000 and 1000 for smaller and larger systems, respectively.

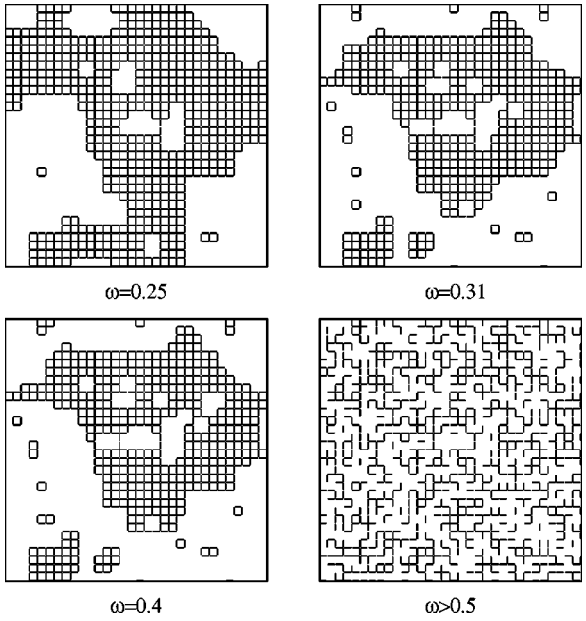

FIG. 1. Typical optimal configurations for different values of ω calculated with the same disorder realization for $w_{ij}(=\pm\omega)$.

A. Results at the critical point

First, we tested the relative accuracy of the two methods by comparing the value of the obtained cost functions, F_0, for different finite sizes. As a general tendency simulated annealing has given lower, thus better estimates, but the relative difference for $L\leqslant 16$ was very small, less then 0.4%. For the largest system we studied by simulated annealing, $L=24$, the relative difference has increased to about 0.6%. We shall later analyze consequences of the inaccuracy of the min-cut method in the magnetic properties of the RBPM. In the following illustration we present results that are obtained by the more accurate simulated annealing method.

Typical optimal configurations for different values of ω calculated with the same disorder realization for $w_{ij}(=\pm\omega)$ are presented in Fig. 1. The position of the strong bonds $(w_{ij}=+\omega)$ can be obtained from the optimal configuration for $\omega>1/2$, since in percolation only these bonds are occupied. As seen in the figure for smaller disorder parameter the optimal graph looks to be more compact, whereas for stronger ω the optimal configurations are very close to each other. This fact is a consequence of the presence of a finite length scale in the problem. As shown in the Appendix for small ω the system behaves uniformly up to a length scale, l_c, which is estimated as

$$l_c \sim \left(\frac{1}{2\omega}\right)^2. \tag{3.4}$$

To observe the true asymptotic behavior in the RBPM calculation the system size should be larger than this value, $L>l_c(\omega)$, therefore we restricted ourselves to not too small ω values.

Next we analyze the distribution of the largest connected cluster, Γ. Inspecting the structure of a typical optimal graph in Fig. 1 we arrive to the conclusion that Γ is a fractal, so

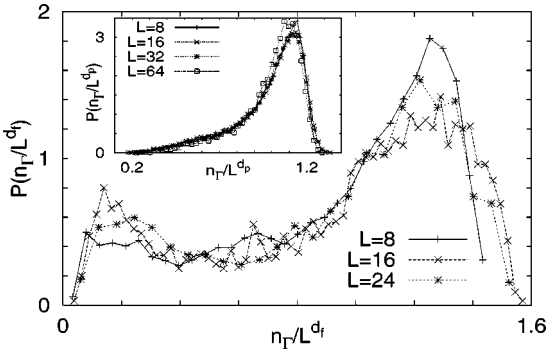

FIG. 2. Scaling plot of the reduced size distribution of the largest cluster at the critical point of the RBPM at $\omega=0.4$ for different finite systems. A data collapse is obtained with an average mass exponent of $d_f\approx 1.8$. In the inset the same quantity is plotted for percolation, when $\omega>1/2$ and $d_p=91/48$.

that we take the scaling combination n_Γ/L^{d_f}, which corresponds to the form in Eq. (2.7). In Fig. 2 we present a scaling plot of the reduced cluster-size distribution, where a data collapse can be obtained with an average mass exponent of $d_f\approx 1.8$.

We note that the points, corresponding to the smallest system, deviate more from the hypothetical scaling curve, which can be attributed to the effect of the finite length scale, l_c. In the inset of Fig. 2 a similar scaling plot is presented in the percolation region, i.e., for $\omega>1/2$, where the fractal dimension of percolation [20], $d_p=91/48$ is used. The scaling curves for $\omega<1/2$ and $\omega>1/2$ look different. For the RBPM the distribution is broad and there is a considerable weight for small clusters, whereas for percolation the distribution is single peaked without a relevant small cluster contribution.

Next we calculate the average density of the largest connected cluster, $[n_\Gamma]_{\rm av}/L^2$, from the size dependence of which the average mass exponent, d_f in Eq. (2.7) and the magnetization exponent, x_m in Eq. (2.10) follows. In Fig. 3 we have plotted $[n_\Gamma]_{\rm av}/L^2$ for different finite sizes in a log-log scale, using different values of the disorder parameter, ω. In this figure, besides the results obtained by simulated annealing, also points calculated by the approximate (min-cut) optimization algorithm are presented. As seen the min-cut algorithm works satisfactory for small systems, $L\leqslant 16$, when the difference in the cost-functions calculated by the two methods is also very small. For larger sizes, however, which are beyond the possibilities of simulated annealing, the error of the optimization algorithm increases. Based on the results presented in Fig. 3 the min-cut method tends to generate a *compact cluster* in the large system limit. Therefore we used the min-cut method only for limited sizes, which are anyhow manageable by the simulated annealing method, although with much longer computational time.

Returning to the average density in Fig. 3 one can observe that for the disorder parameter in the RBPM range, i.e., $0<\omega<1/2$, the points fall on nearly parallel straight lines having a slope of $-2+d_f\simeq -0.2$, where $d_f\simeq 1.8$ corresponds to the value we used in the scaling plot of the reduced cluster-size distribution in Fig. 2. The slope of the same line calculated in the percolation regime, with $\omega>0.5$ is significantly

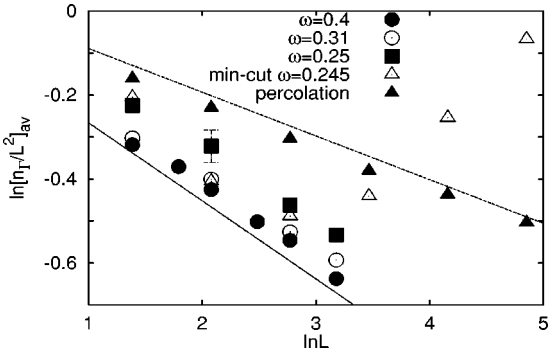

FIG. 3. Size dependence of the average density of the largest connected cluster at different values of the disorder parameter ω, calculated by simulated annealing and by the approximative optimization (min-cut) algorithm. Note that the min-cut method has a systematic error for larger systems. The slope of the curves, s, for different $0<\omega<0.5$ is approximately identical and indicated by a straight line with $s=-0.2$, but this slope differs from that of percolation, which corresponds to $\omega>0.5$, and the related straight line has $s=-5/48$, the typical error of the simulated annealing method is indicated by the error bar, whereas the error for percolation is smaller than the size of the symbol.

different, it is $-2+d_p\simeq-0.1$, where d_p is close to the fractal dimension of 2D percolation.

The estimates of the magnetization scaling dimension, x_m, in Eq. (2.10) at different disorder parameter, ω, are summarized in Table I.

As seen in Table I the average magnetization exponent, x_m, is approximately independent of the disorder parameter for $0<\omega<1/2$, and its value is within the range of $x_m \approx 0.17$–0.19. This is in agreement with the estimates obtained by extrapolating the results calculated at finite q's [14,15], thus the two limits seem to be interchangeable. The apparent variation of x_m with ω can be attributed to crossover effects. At $\omega=0$ the pure system transition, whereas at $\omega=1/2$ the percolation fixed point is going to perturb the value of effective, finite-size-dependent exponents.

The average magnetization exponent, x_m, has been calculated by another method, which is based on conformal invariance [19]. Here we use the result, that in a long strip of width, L_w, and with periodic boundary conditions the average correlation function along the strip decays exponentially

$$[\langle\sigma_i\sigma_{i+u}\rangle]_{\mathrm{av}}\sim\exp(-u/\xi_{L_w}), \tag{3.5}$$

TABLE I. Scaling exponent, x_m, of the average magnetization for different disorder parameter, ω. The last row with $\omega>0.5$ corresponds to normal percolation where the exact value is $x_m^p=5/48=0.104$.

ω	x_m
0.2	0.185(30)
0.25	0.188(16)
0.31	0.165(15)
0.4	0.178(13)
>0.5	0.103(2)

TABLE II. Numerical estimates for the average magnetization exponent, x_m, using the correlation length-exponent relation in Eq. (3.6) for different widths, L_w.

	x_m			
ω	$L_w=2$	$L_w=3$	$L_w=4$	$L_w=5$
0.400	0.263(9)	0.166(4)	0.165(5)	0.163(6)
0.423	0.267(1)	0.168(5)	0.167(2)	0.163(6)
0.452	0.266(1)	0.170(4)	0.169(2)	0.163(6)

where the correlation length, ξ_{L_w}, for large widths asymptotically behaves as

$$\xi_{L_w}=\frac{L_w}{2\pi x_m}. \tag{3.6}$$

In practical calculations we used strips of widths, $L_w=2$, 3, 4, and 5, and with such a lengths that in the calculated correlation function the exponential decay in Eq. (3.5) does not seem to change by further increase of the length. Generally we went at least up to a length of 64 sites, which has then limited the available widths, L_w. The calculated exponents for some values of the disorder parameter are given in Table II.

As seen in Table II the size dependence of x_m is very weak for $L_w\geqslant 3$ and the extrapolated value of $x_m\simeq 0.17$ is practically independent of the form of the disorder. This estimate is compatible with the previous one obtained by finite-size scaling. The fact, that this latter result lies close to the lower bound of the finite-size scaling one is probably due to the confluent singularity of the percolation fixed point, which is quite strong in the region of ω's we used in the calculation on strips.

We have also calculated the central charge of the conformal anomaly, c, from the finite-size correction to the free energy per width

$$f_0(L_w)=f_0(\infty)-\frac{\pi c}{6L_w^2}+O(L_w^{-3}), \tag{3.7}$$

with the result

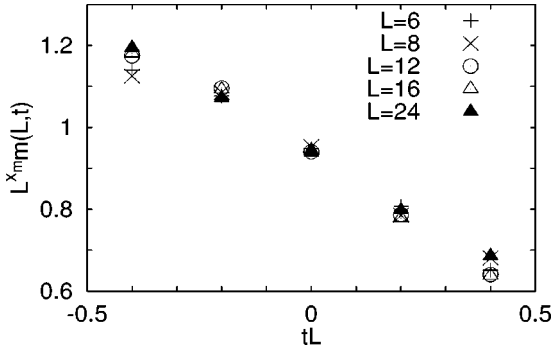

FIG. 4. Scaling plot of the finite-size average magnetization in the vicinity of the critical point, for a disorder parameter $\omega=0.4$. The scaling exponents we used here are $x_m=0.177$ and $\nu=1$.

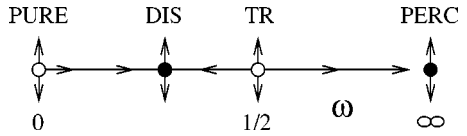

FIG. 5. Schematic RG phase diagram of the 2D RBPM with varying strength of bimodal disorder, ω. For details see the text.

$$c = 0.74(1) = \frac{0.51(1)}{\ln 2}. \tag{3.8}$$

This is compatible with previous estimate [15] $c \simeq 0.5/\ln 2$, which is obtained by finite-q extrapolation.

B. Results outside the critical point

We close our paper by an investigation of the average magnetization, $[m(L,t)]_{\rm av}$, in the vicinity of the critical point. In the scaling region, defined as $L|t|^{\nu} = O(1)$, where ν is the critical exponent of average correlations, the average magnetization is expected to behave as

$$[m(L,t)]_{\rm av} = L^{-x_m} \tilde{m}(L|t|^{\nu}), \tag{3.9}$$

where $\tilde{m}(y)$ is some scaling function. The calculated magnetizations at different finite size and temperature then should collapse to the same scaling function, provided the correct critical exponents, x_m and ν are used. In Fig. 4 we show the result of such a scaling plot, where we used $\nu = 1$, as found approximately in finite-q calculations, whereas for x_m we used our previous estimate obtained through finite-size scaling at the critical point. The data collapse in Fig. 4 is satisfactory, however, to obtain a precise estimate on ν one needs to extend the calculations for larger systems.

IV. DISCUSSION

In this paper the critical behavior of the Potts model with nonfrustrated, random couplings is studied in the large-q limit. We have shown how the calculation of the free-energy and the correlation functions of the RBPM can be mapped onto an optimization problem, which is then studied by simulated annealing and by an approximate combinatorial optimization algorithm. Working with the bimodal distribution in Eq. (2.11) our results are compatible with the renormalization group (RG) phase diagram drawn in Fig. 5.

The pure systems fixed point, situated at $\omega = 0$, is unstable against any weak disorder, thus the critical behavior in the range of $0 < \omega < 0.5$ is controlled by the disordered fixed point (DIS). Our numerical calculation indeed indicate a universality with respect of the strength of disorder. Increasing the disorder over $\omega = 0.5$ we reach the region of attraction of the normal percolation, and the corresponding fixed point (PERC) is located at $\omega = \infty$. Our RG phase diagram is completed by introducing a repulsive tricritical fixed point, TR, at $\omega = 0.5$, which separates the regions of attraction of the two nontrivial fixed points, DIS and PERC. The singular properties of the TR can be quite unusual, since the corresponding optimal graph is highly degenerate. The possible configurations include all that interpolate between that of the RBPM and that of normal percolation.

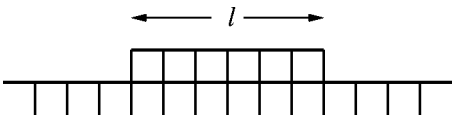

FIG. 6. A connected cluster with a step of l points on the top of a straight surface.

The behavior of the system at the fixed-point DIS, which is the subject of the present paper, is strongly dominated by disorder effects, whereas thermal fluctuations seem to be negligible. Similar, disorder dominated critical behavior occur in random quantum spin chains, where analytical results are available [21–23], and also in 2D random quantum ferromagnets [24]. Whether exact results can be obtained also for the 2D RBPM in the large-q limit will be seen in future research.

ACKNOWLEDGMENTS

F.I. is grateful to J-C. Anglés d'Auriac and L. Turban for useful discussions. This work has been supported by a German-Hungarian exchange program (DAAD-MÖB), by the Hungarian National Research Fund under Grant No. OTKA TO23642, TO25139, TO34183, MO28418, and M36803, and by the Ministry of Education under Grant No. FKFP 87/2001.

APPENDIX: LENGTH SCALE IN THE SMALL DISORDER LIMIT

Here we estimate the size, l, of a step, which is situated at the top of a straight surface of a connected cluster, see Fig. 6. Using the bimodal distribution in Eq. (2.11) the existence of the step is connected to the condition

$$\sum_{i=1}^{2l-1} \left(\frac{1}{2} + w_i \right) > l, \tag{A1}$$

where $w_i = \pm\omega$ with the same probability, or equivalently

$$\sum_{i=1}^{2l-1} p_i > \frac{1}{2\omega}, \tag{A2}$$

with $p_i = \pm 1$. For large l the probability distribution of the sum in the left-hand side of Eq. (A2) is Gaussian, with a variance of $\sqrt{2l-1}$. Consequently the average size of the step, l_c, scales with a small ω as

$$l_c \sim \left(\frac{1}{2\omega} \right)^2, \tag{A3}$$

as given in Eq. (3.4).

[1] A.B. Harris, J. Phys. C **7**, 1671 (1974).
[2] J.T. Chayes, L. Chayes, D.S. Fisher, and T. Spencer, Phys. Rev. Lett. **57**, 2999 (1986).
[3] A.W.W. Ludwig, Nucl. Phys. B **285**, 97 (1987); **330**, 639 (1990); A.W.W. Ludwig and J.L. Cardy, *ibid.* **330**, 687 (1990); Vl. Dotsenko, M. Picco, and P. Pujol, *ibid.* **455**, 701 (1995); M.A. Lewis, Europhys. Lett. **43**, 189 (1998).
[4] M. Aizenman and J. Wehr, Phys. Rev. Lett. **62**, 2503 (1989).
[5] Y. Imry and M. Wortis, Phys. Rev. B **19**, 3580 (1979).
[6] K. Hui and A.N. Berker, Phys. Rev. Lett. **62**, 2507 (1989).
[7] For a recent numerical study about the 3D random-Potts model see C. Chatelain, B. Berche, W. Janke, and P.E. Berche, e-print cond-mat/0103377.
[8] W. Kinzel and E. Domany, Phys. Rev. B **23**, 3421 (1981).
[9] R.J. Baxter, J. Phys. C **6**, L445 (1973).
[10] S. Chen, A.M. Ferrenberg, and D.P. Landau, Phys. Rev. Lett. **69**, 1213 (1992); Phys. Rev. E **52**, 1377 (1995); S. Wiseman and E. Domany, *ibid.* **51**, 3074 (1995).
[11] M. Kardar, A.L. Stella, G. Sartoni, and B. Derrida, Phys. Rev. E **52**, R1269 (1995).
[12] M. Picco, Phys. Rev. Lett. **79**, 2998 (1997); C. Chatelain and B. Berche, *ibid.* **80**, 1670 (1998); Phys. Rev. E **58**, R6899 (1998); **60**, 3853 (1999); G. Palágyi, C. Chatelain, B. Berche, and F. Iglói, Eur. Phys. J. B **13**, 357 (2000).
[13] J.L. Cardy and J.L. Jacobsen, Phys. Rev. Lett. **79**, 4063 (1997); J.L. Jacobsen and J.L. Cardy, Nucl. Phys. B **515**, 701 (1998).
[14] T. Olson and A.P. Young, Phys. Rev. B **60**, 3428 (1999).
[15] J.L. Jacobsen and M. Picco, Phys. Rev. E **61**, R13 (2000).
[16] P.W. Kasteleyn and C.M. Fortuin, J. Phys. Soc. Jpn. **46** (Suppl.), 11 (1969).
[17] At the critical point the dominant graph is generally not unique, cf. with the bimodal distribution in Eq. (2.11) any two clusters having just one strong and one weak bond between them could be either connected or disconnected. We assume that the degenerate optimal graphs have the same asymptotic fractal properties.
[18] T. Hagerup (unpublished).
[19] See, e.g., J.L. Cardy, in *Phase Transitions and Critical Phenomena*, edited by J.L. Lebowitz and M.S. Green (Academic, London, 1987), Vol. 11, p. 1.
[20] D. Stauffer and A. Aharony, *Introduction to Percolation Theory* (Taylor & Francis, London, 1992).
[21] D.S. Fisher, Phys. Rev. Lett. **69**, 534 (1992); Phys. Rev. B **51**, 6411 (1995).
[22] F. Iglói and H. Rieger, Phys. Rev. B **57**, 11 404 (1998).
[23] F. Iglói, R. Juhász, and P. Lajkó, Phys. Rev. Lett. **86**, 1343 (2001).
[24] O. Motrunich, S.-C. Mau, D.A. Huse, and D.S. Fisher, Phys. Rev. B **61**, 1160 (2000); Y-C. Lin, N. Kawashima, F. Iglói, and H. Rieger, Prog. Theor. Phys. Suppl. **138**, 470 (2000).